ADVANCED MATERIALS TECHNOLOGIES
www.advmattechnol.de

Chemical Doping of the Organic Semiconductor C8-BTBT-C8 Using an Aqueous Iodine Solution for Device Mobility Enhancement

Jinghai Li, Adara Babuji, Inés Temiño, Tommaso Salzillo, Francesco D'Amico, Raphael Pfattner, Carmen Ocal, Esther Barrena, and Marta Mas-Torrent**

The performance of organic field-effect transistors is still severely limited by factors such as contact resistance and charge trapping. Chemical doping is considered to be a promising key enabler for improving device performance, although there is a limited number of established doping protocols as well as a lack of understanding of the doping mechanisms. Here, a very simple doping methodology based on exposing an organic semiconductor thin film to an aqueous iodine solution is reported. The doped devices exhibit enhanced device mobility, which becomes channel-length independent, a decreased threshold voltage and a reduction in the density of interfacial traps. The device OFF current is not altered, which is in agreement with the spectroscopic data that points out that no charge transfer processes are occurring. Kelvin probe force microscopy characterization of the devices under operando conditions unambiguously proves that an important reduction of the contact resistance takes place after their exposition to the iodine solution, reaching almost ohmic contact.

1. Introduction

Organic semiconductor (OSC) thin films have been widely used as active materials in devices ranging from organic light-emitting diodes (OLEDs), solars cells, thermoelectrics or sensors, among others.[1–3] In particular, organic field-effect transistors (OFETs) represent ideal devices to investigate the transport properties of OSCs, and are also of high interest for a wide range of low-cost, flexible and large-area applications.[4,5] Over the past few years, an impressive improvement in OFET performance combined with the appearance of novel OSC roll-to-roll compatible printing techniques, have pushed forward the application potential of organic electronics.[6–8] Despite these encouraging results, the performance of OFETs is still severely limited by factors such as contact resistance (R_c)[9] and charge trapping.[10]

When the highest occupied molecular orbital (HOMO) or the lowest unoccupied molecular orbital (LUMO) of a p-type or n-type OSC, respectively, and the electrodes work-function are not aligned, charge injection is significantly hindered by the high energy barrier and high contact resistance values are extracted.[11] In order to confront these issues, different electrode engineering approaches have been proposed. For example, the work-function of the metal electrodes can be modified to match the OSC energy level by using self-assembled molecular monolayers (SAMs) in bottom-contact devices or by inserting a charge injection layer in top-contact OFETs.[12–14]

Another source that prevents OSCs from realizing their instrinsic charge carrier mobilities is charge trapping. In the energy gap of OSCs, electronic states can appear due to the presence of chemical impurities or defects that trap mobile charge carriers, thus causing OFETs to deviate from the ideal behavior.[15] It has been previously reported that passivation of the dielectric layer or the use of OSC:insulating polymer blends are appealing routes to decrease the dielectric interfacial trap density.[16] Nonetheless, traps are also present at the metal–OSC interface, grain boundaries and thin film structural inhomogeneities.[15]

Chemical doping is a suitable way to modify the electronic properties of OSCs, which consists in adding a small percentage of species able to donate (n-doping) or accept (p-doping) an electron to or from the OSC, respectively. Doping of semiconductors is a well-established strategy in inorganic transistors with great success also in organic optoelectronics, especially in OLEDs and solar cells.[17–22] Regarding OFET devices, doping has mainly been exploited to increase device mobility, adjust the threshold voltage, fill up trap states, or to improve charge injection by contact doping.[23] Although recent works have demonstrated that doping can be a key enabler for high performing OFETs, the progress of organic semiconductors doping is still

J. Li, A. Babuji, I. Temiño, T. Salzillo, R. Pfattner, C. Ocal, E. Barrena, M. Mas-Torrent
Institut de Ciència de Materials de Barcelona
ICMAB-CSIC
Campus UAB, Bellaterra 08193, Spain
E-mail: ebarrena@icmab.es; mmas@icmab.es
F. D'Amico
Elettra Sincrotrone Trieste S.C.p.A.
S.S. 14 km 163,5 in Area Science Park, Basovizza TS 34149, Italy
The ORCID identification number(s) for the author(s) of this article can be found under https://doi.org/10.1002/admt.202101535.

DOI: 10.1002/admt.202101535

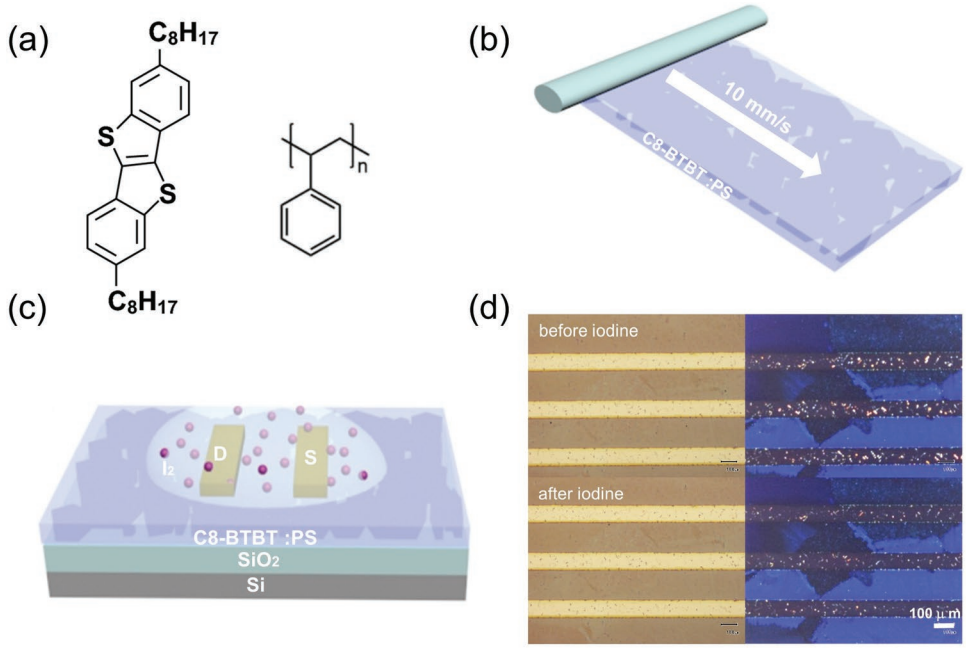

Figure 1. a) Chemical structures of C8-BTBT-C8 and PS. b) Schematic illustration of the BAMs technique. c) Scheme of the device and doping methodology. d) Optical microscopy and polarized optical microscopy images of C8-BTBT-C8:PS thin films before and after iodine doping .

hindered by the limited number of established doping protocols as well as by the lack of understanding the doping mechanisms.

Doping in OFETs has been realized employing thermal evaporation,[24–26] solution-based processes,[27–30] and physisorption.[31] The latter category includes the p-type doping by exposure with oxidizing gases such as iodine, which was already investigated as dopant for polyacetylene films in the 1970s and later applied to pentacene single crystals and thin films.[32] However, although exposing the semiconductor layer to dopant vapors is technically simple, this methodology lacks control over the doping level. As an alternative, we recently reported a route to dope an OSC surface by exposing it to an aqueous solution containing Hg^{2+}.[33] In that case, a redox reaction between mercury ions and the semiconductor surface led to a threshold voltage shift in water-gated OFETs.

OFETs based on the organic semiconductor 2,7-dioctyl[1]benzothieno[3,2-b][1]benzothiophene (C8-BTBT-C8)(**Figure 1**a) have demonstrated to exhibit remarkable field-effect mobilities.[4,34–36] However, large negative threshold voltage values and high contact resistances have been often encountered, most likely as a result of the energy mismatch at the organic–metal interface, compelling the search of contact optimization strategies.[26,37–39] Here, we report on a very simple doping methodology based on exposing a solution sheared C8-BTBT-C8 thin film to an aqueous iodine solution. As evidenced by macroscopical electrical measurements and local Kelvin probe force microscopy (KPFM) characterization, this strategy leads to devices with a strong improvement of the injection properties and overall electrical characteristics. The doped devices exhibit enhanced device mobility and decreased threshold voltage, without altering the OFF current. In addition, the impact of iodine on the OFET electrical performance can be modulated with the concentration of the iodine solution. We elucidate that the significant reduction of the contact resistance is the major achievement of our doping strategy.

2. Results and Discussion

2.1. Effect of Iodine Doping on the Electrical Characteristics

Thin films of blends of C8-BTBT-C8 and polystyrene (PS) in a ratio 4:1 were prepared on SiO_2 substrates employing the bar-assisted meniscus shearing technique (BAMS, Figure 1b), as previously reported.[4,40] The use of blends combined with the deposition by BAMS has shown to lead to crystalline films over large areas at high throughput. Gold top source–drain contacts were thermally evaporated through a shadow mask consisting of device motifs with identical channel width (W) but with different channel lengths (L) (see Experimental Section).

For chemical doping, the surface of the OSC film was exposed to an aqueous iodine solution for 3 min (see Figure 1c for a scheme illustrating the doping methodology followed). As discussed in detail below, iodine exposure resulted in an increase in the field-effect mobility and a positive shift of the threshold voltage (V_{th}). The influence of the iodine solution concentration on the device electrical characteristics was evaluated by exposing the films to an increasingly concentrated iodine solution. We observed a mobility and V_{th} shift increase in the range of 0.0013–0.010 mg mL^{-1} (**Figure 2**: Figures S1 and S2, Supporting Information). Further increase in the iodine concentration led to a small decrease followed by the stabilization of these parameters. Therefore, the device electrical response can be controlled by tuning the iodine concentration. Although higher mobility values are achieved at lower iodine concentrations, all the experiments performed below were carried out exposing the devices with more concentrated solutions (i.e., 0.29 mg mL^{-1}) in order to achieve more reproducibility. Note that increasing exposure time did not further affect the device mobility (Figure S3, Supporting Information).

The C8-BTBT-C8:PS thin films were inspected before and after iodine exposure by polarized optical microscopy and X-ray

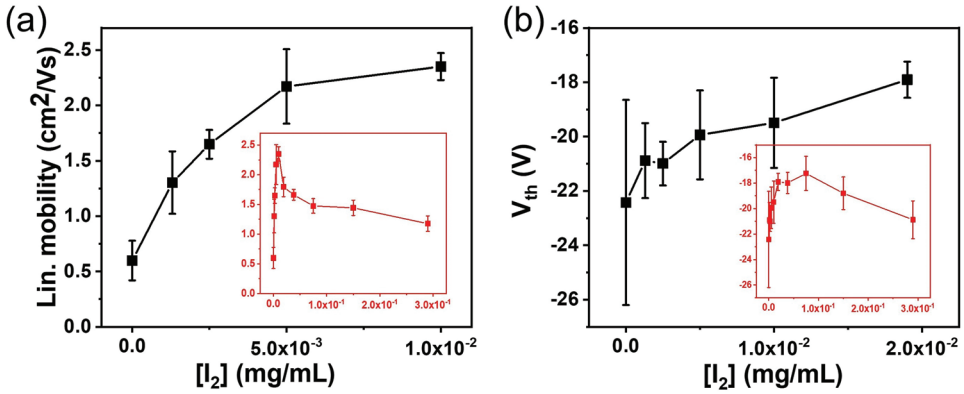

Figure 2. a) Linear mobility and b) linear threshold voltage dependence of a short channel length OFET (35 µm) with the concentration of iodine water solution. Data extracted from three films exposed to an increasingly concentrated iodine solution. Each point on the plot represents the mean value and the error bar corresponds to the standard deviation of the data.

diffraction. As it can be observed in Figure 1d, the thin films exhibit a polycrystalline structure with large lateral sizes (hundreds of micrometers), which do not experience major visible changes after the doping process. Moreover, the diffraction patterns of the pristine and doped films are identical (Figure S4, Supporting Information), meaning that the crystallinity of the films is not affected. Three diffraction peaks (001, 002, and 003) located at 3.01°, 6.13°, and 9.16° were observed, indicating that films are oriented with the *ab* plane parallel to the substrate surface. From these data, a *d*-spacing of 2.90 nm was calculated, which is in agreement with the length of an extended C8-BTBT-C8 molecule and with the previously reported single-crystal structure for this material.[39,41]

The effect of the iodine treatment on the OFETs electrical performance was carefully examined in devices with different channel lengths (**Figure 3**; Figures S5–S7, Supporting Information). The pristine devices exhibit a mobility with a considerably strong dependence on channel length (**Table 1** and Figure 3c; Figure S5, Supporting Information). The longest channel devices exhibit a high hole mobility of 1.75 $cm^2\ V^{-1}\ s^{-1}$

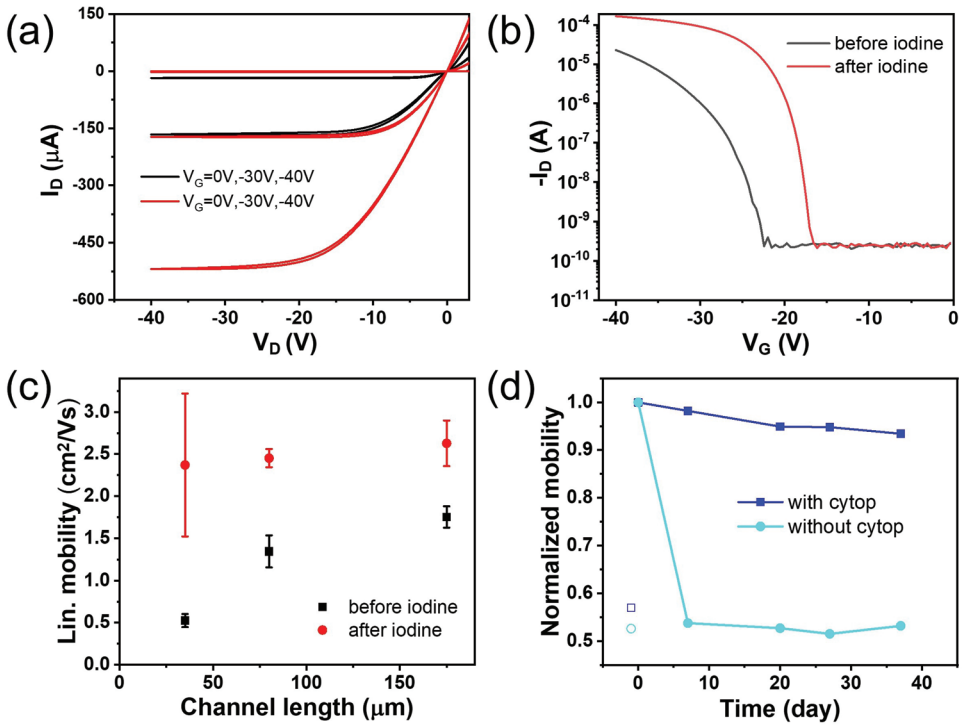

Figure 3. a) Representative output curves corresponding to the OFETs before (black) and after (red) iodine water solution exposure (W = 4000 µm, L = 35 µm), and b) linear transfer curves of the same device ($V_D = -5$ V). c) Linear mobility for OFET devices of different lengths (L = 35 ± 5, 80 ± 5, and 175 ± 5 µm) before and after exposure to the iodine water solution. Each point on the plot represents the mean value of four devices and the error bar corresponds to the standard deviation of the data. d) Normalized linear mobility evolution with time of devices exposed to iodine water solution with and without a Cytop encapsulation layer. Notice that the initial mobility values (empty symbols) correspond to the undoped devices.

Table 1. Electrical characteristics extracted for undoped (doped) devices with different channel lengths.

Channel length	35 µm	80 µm	175 µm
$\mu_{lin.}$ [$cm^2\ V^{-1}\ s^{-1}$]	0.53 ± 0.08 (2.37 ± 0.85)	1.35 ± 0.19 (2.45 ± 0.11)	1.75 ± 0.13 (2.63 ± 0.27)
Lin. V_{th} [V]	−33 ± 0.3 (-22 ± 0.8)	−32 ± 1.2 (−21 ± 2.0)	−32 ± 0.4 (−25 ± 0.6)
SS [$V\ dec^{-1}$]	1.34 ± 0.23 (0.76 ± 0.10)	1.26 ± 0.26 (0.80 ± 0.17)	1.37 ± 0.23 (0.81 ± 0.10)
N_t [$10^{12}\ eV^{-1}\ cm^{-2}$]	2.33 ± 0.40 (1.28 ± 0.17)	2.19 ± 0.45 (1.35 ± 0.29)	2.39 ± 0.40 (1.37 ± 0.17)

in the linear regime, while for the shortest-channel ones the mobility drops by more than three times (i.e., 0.53 $cm^2\ V^{-1}\ s^{-1}$). Such a non-ideal behavior can be explained in terms of the large weighted contribution of the contact resistance at short channel lengths, where the channel resistance ($R_{channel}$) is smaller. As already reported, the performance of this type of devices is strongly contact-limited,[26,42] resulting in OFET mobilities much below the intrinsic value of this OSC.

After exposure to the iodine solution, a higher source–drain current was measured in both output and transfer electrical characteristics, being the maximum ON current about one order of magnitude higher compared to the pristine devices. Remarkably, both linear and saturation mobility became channel-length independent, with the linear mobility increasing up to around 2.5 $cm^2\ V^{-1}\ s^{-1}$ (Table 1 and Figure 3c; Figure S5, Supporting Information). In addition, V_{th} was positively shifted from –31 V in the pristine devices to –20 V after iodine exposure. Given that V_{th} is the gate–source voltage required for compensating immobile charges present at the organic–dielectric interface to form the charge accumulation layer, the observed V_{th} shift is a proof of trap filling upon the OSC exposure to the iodine solution.[17,43]

The interfacial charge trap density per unit area (N_t) can be calculated from the subthreshold swing (SS) according to:

$$SS = \frac{\partial V_G}{\partial(\log I_D)},\ N_t = \frac{C}{e^2}\cdot\left[\frac{e\cdot SS}{k_B\cdot T\cdot ln10} - 1\right] \quad (1)$$

where e is the electron charge, k_B is the Boltzmann constant, C is the capacitance per unit area of the dielectric (C = 17.26 nF cm^{-2}) and T the absolute temperature. V_G and I_D stand for the applied gate voltage and the measured drain current, respectively. Table 1 collects the N_t values extracted for the pristine and doped films in the linear regime. For all channel-length devices, there is a clear reduction in the interfacial trap density, from values around 2.3×10^{12} $eV^{-1}\ cm^{-2}$ in the pristine devices down to around 1.3×10^{12} $eV^{-1}\ cm^{-2}$ in the doped ones. This decrease indicates that trap states filling is a beneficial effect resulting from the iodine doping treatment.

It should be noticed that the OFF current does not increase after the doping treatment (Figure 3b), indicating that no free mobile charges are generated in the film, and thus, no redox reaction is taking place. This is in agreement with the electrochemical properties of iodine[44,45] and the deep lying HOMO of C8-BTBT-C8.[46–49] In addition, the UV–vis–NIR spectra of the doped films did not show any charge transfer absorption band confirming that no charge transfer process occurs (i.e., C8-BTBT-C8 is not oxidized; Figure S8, Supporting Information). Further, it is known that from the edge of the lowest energy absorption band it is possible to estimate the HOMO–LUMO bandgap.[50] Since there are no appreciable changes in the spectra before and after doping, we can affirm that the energy bandgap in the C8-BTBT-C8 films, and, hence, the organic semiconductor HOMO level, is not modified after doping. The absence of changes in the electronic configuration of C8-BTBT-C8 was also verified by the comparison between the UV Resonant Raman (UVRR) spectra of C8-BTBT-C8 before and after the iodine treatment (**Figure 4**). The Raman spectra do not show any shift relative to the normal modes at 1471, 1550, and 1595 cm^{-1} (thiophene rings, ring stretching), thus further excluding important charge transfer phenomena.

To rule out any effect arising from the water influence on the organic semiconductor thin film, we characterized a device before and after exposure only to MilliQ water for 3 min. The corresponding output and transfer characteristics as well as the morphology of those films are shown in Figure S9 (Supporting Information). It was observed that the films were neither electrically nor morphologically affected by water, confirming that iodine is the solely responsible for the changes observed in the electrical characteristics of the doped devices. Indeed, as it will be demonstrated in the following, the amelioration of the devices' performance is caused by the positive effect of iodine on the contact resistance.

Iodine doping is known to be rather unstable over time since iodine tends to desorb in ambient conditions due to its very low

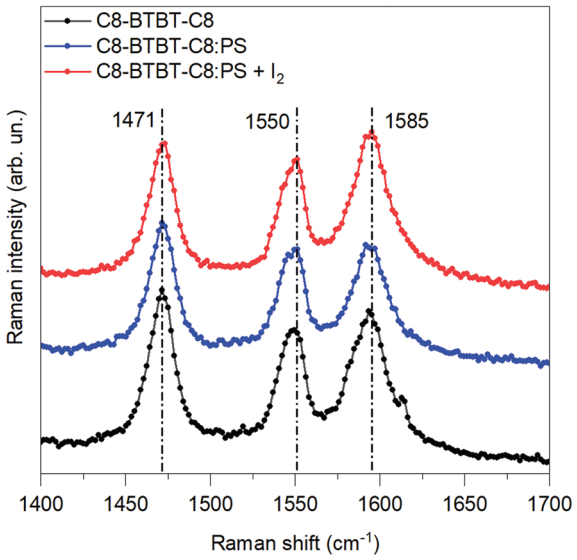

Figure 4. UV Resonant Raman spectra (excitation wavelength 266 nm) of a C8-BTBT-C8 film (black curve) and C8-BTBT-C8:PS blend before doping (blue curve) and after exposure to iodine water solution (red curve).

vapor pressure (around 40 Pa at room temperature). Hence, the stability of iodine-doped devices was checked (Figure 3d). Unsurprisingly, the mobility of doped devices decreased to values close to their initial ones after 1 week. However, doped devices that were encapsulated with a spin coated Cytop layer, only showed a 10% decrease of mobility after 37 days.

2.2. OSC–Electrode Interface: Contact Resistance and Microscopic Effects

In order to evaluate the impact of the iodine doping approach on the contact resistance, the device electrodes and channel were inspected by KPFM. The corresponding data before doping (left column) and after doping (right column) are presented in **Figure 5**. Magnified images at the channel before the doping process (inset in Figure 5a) show that the C8-BTBT-C8:PS film exhibits a very smooth surface (rms ≈ 0.7 nm) consisting of terraces and some parallel grooves. Height analysis by atomic force microscopy (AFM) gives a total film thickness of ≈15 nm and grooves depth of ≈10 nm, indicating the presence of a PS-rich continuous film at the film bottom, as discussed in detail elsewhere.[23] The height of the terraces corresponds to the expected 3 nm spacing between C8-BTBT-C8 layers (see above). To have a microscopic view of the consequences derived from iodine on the OFET, we have evaluated the electrostatic potential profile across the devices by KPFM under operation conditions by varying drain voltage (V_D) and gate voltage (V_G). Two sets of data were acquired for diverse V_D (–1 to –5 V) at fixed V_G = –20 V and for diverse V_G (–20 to –40 V) at fixed V_D = –1 V. Figure 5c,d shows typical potential profiles obtained for a pristine OFET. The simultaneously measured topographic profile (Figure 5b) permits differentiating the channel region from the electrodes (indicated by vertical black dashed lines) and, therefore, determining the actual distance between gold pads (≈27 µm for this particular OFET). For clarity, Figure 5c only displays the potential profile for V_G = –40 V (V_D = –1 V), corresponding to the linear regime operation for this OFET. As expected, there is a strictly linear decay of the potential across the channel. However, a significant potential drop is measured at the source (S) and drain (D), which is attributed to the electrodes/OSC contact resistance (R_S and R_D, respectively), indicating an energy barrier for charge injection. The total contact resistance ($R_C = R_S + R_D$) is 10 kΩ cm. The ratio of the contact resistance to the total resistance ($R_T = V_D/I_D$) is R_C/R_T = 0.66, indicating that the OFET electrical performance is dominated by the contact resistance. The contact effects are also clearly observed for potential profiles as a function of V_D while the gate voltage was kept constant at V_G = –20 V (Figure 5d). For these operation conditions, where the gate voltage is close to V_{th}, the largest contact resistance is at the source electrode. The potential profiles for all V_G values analyzed (–20 to –40 V) as well as the corresponding R_C are provided in Figure S10 (Supporting Information). The contact resistance manifestly depends on the gate bias, being larger for decreased V_G. This fact is commonly observed in OFETs and may have distinct causes (gated Schottky barrier, gate-dependent mobility, trapping, etc.).[10]

The data collected from the same device upon exposure to the iodine water solution (right column in Figure 5), shows two notorious differences. First, it is outstandingly observed that the potential drop at both contacts almost vanished (Figure 5g,h), indicating that doping has indeed led to a strong reduction of the contacts' resistance. In fact, given how small it is, an accurate calculation of the potential drop above the noise level is not possible for the OFET operating in linear regime (Figure 5g). We can therefore conclude that upon doping there is a negligible contribution of R_C, explaining the ideal behavior of the macroscopic electrical characteristics and the independence of the effective field effect mobility on the channel length. Second, another key feature is observed when comparing the simultaneously measured topographic and potential profiles. Whereas in the pristine case, the edges of each electrode coincide in topographic and potential profiles (see vertical lines in Figure 5b,c), they do not coincide after doping. While the same distance between electrodes is measured in topography before and after the treatment (black dashed lines separated by 27 µm in Figure 5b,f), the linear decay of the electrostatic potential extends over a larger region (vertical blue dashed lines in Figure 5g,h). This visible disagreement indicates that the effective channel length of the doped device is larger than expected and herewith, the device field effect mobility is in fact larger than the calculated value.

Close inspection to the channel (see inset of Figure 5e) shows small aggregates over the surface. Although the nature of such aggregates cannot be determined from the present data, and once discarded any influence of the water itself, we conclude that they are the result of physicochemical effects caused by the aqueous iodine solution. Thus, it is plausible to suggest a certain etching effect of the gold electrode edge that, leading to unconnected metal aggregates, causes its electronic decoupling from the macroscopic electrode.

Summing up, we experimentally observe that the exposure of the OFETs to an aqueous iodine solution results in i) a device mobility increase and ii) a positive V_{th} shift. Both effects are attributed to the reduction of interfacial charge traps density, evidenced by the improvement in the SS. The process leads to higher ON current while leaving unaltered the OFF current, i.e., enhances the ON/OFF ratio. The absence of spectroscopic features typical of charge transfer processes (UV–vis–NIR and Raman) suggest a very low concentration of free charges in the film. Overall, the presented results point to a doping effect at the interfaces as the origin of electrical improvement. Indeed, KPFM proves a strong contact resistance reduction, as the major doping outcome. The improvement of the contact properties may arise from a reduction of the energy barrier at the metal–OSC interface, hence facilitating charge injection. In addition, doping might lead to filling of trap sites at the contact adjacent region, which facilitates charge transport from the electrodes toward the channel, reducing the so-called access resistance.[51,52] The electrostatic potential profiles obtained during operation reveal an effective OFET channel length larger than the topographic one. Although the origin of this event is elusive, it confirms a physicochemical effect of the iodine solution at the metal–OSC interface.

Given that chemical doping by aqueous iodine solution has the benefit of ameliorating the contact properties, a larger increase of effective field effect mobility is observed for those devices limited by the contact resistance (i.e., specially

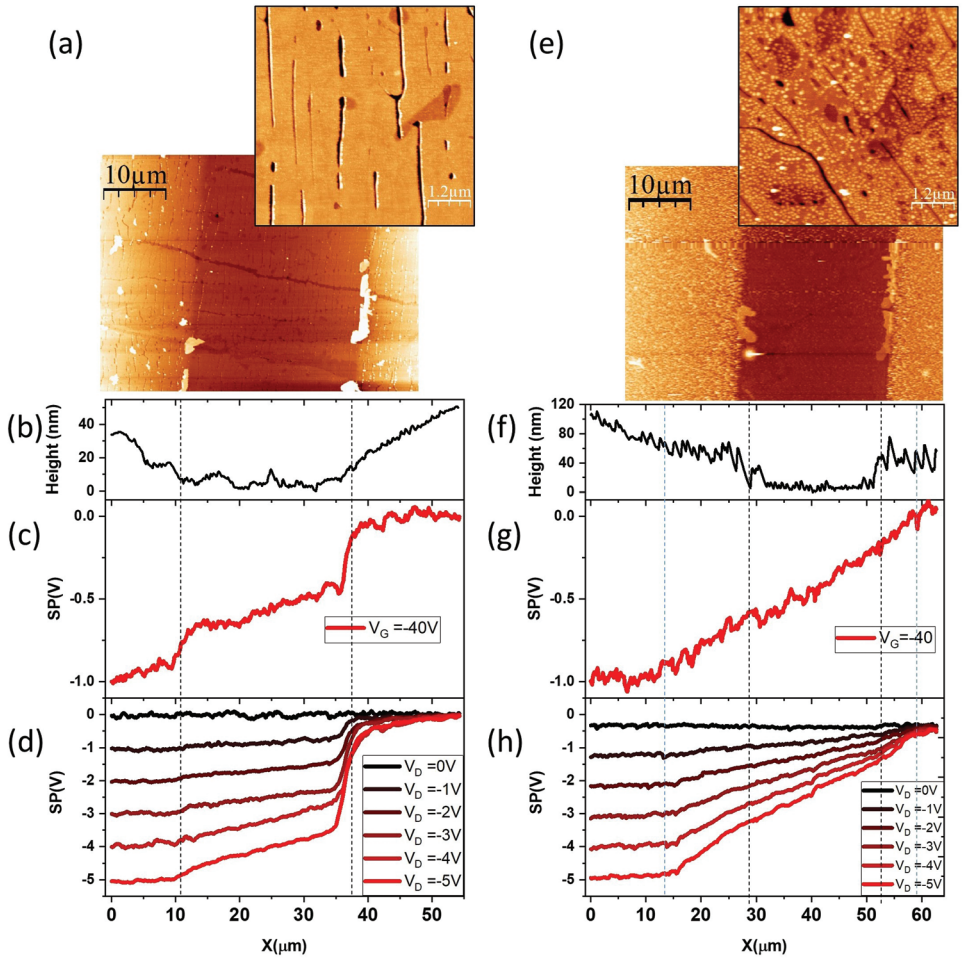

Figure 5. Topographic images of the same C8-BTBT-C8 OFET before (a) and after (e) iodine doping. In the large scan images, the dark middle region corresponds to the device channel and the lighter areas (left and right to the channel) to the Au top contacts. Insets in (a) and (e) are magnification images to show morphological details within the channel. The corresponding topographic profiles, shown in (b) and (f), include part of both contacts (delimited by the vertical black dashed lines). The Surface Potential (SP) profiles before and after doping are shown for $V_D = -1$ V and $V_G = -40$ V in (c) and (g) while for $V_G = -20$ and diverse V_D are shown in (d) and (h). Note: the vertical blue dashed lines in (f–g) indicate the distance where the potential drops after doping.

devices with shorter-channel) (Table 1). It should be noted that the same doping procedure was applied in thin films of the benchmark organic semiconductors 6,13-bis(triisopropylsilylethinyl)pentacene (TIPS-Pentacene) and 2,8-difluoro-5,11-bis(triethylsilylethynyl)anthradithiophene (diF-TES-ADT). These materials do not suffer from contact resistance issues since their HOMO level is aligned with the gold work-function.[53,54] Accordingly, the doping procedure did not affect the effective field effect mobility in diF-TES-ADT and TIPS-Pentacene devices (Figure S11, Supporting Information).

3. Conclusion

We demonstrate here that exposing organic semiconducting thin films to an aqueous iodine solution is a fast, reliable, and simple doping method to improve contact effects in OFETs, as proven here in printed C8-BTBT-C8:PS thin films. Importantly, doped devices exhibit a significant enhancement of the field-effect mobility, a positive shift of the threshold voltage and a higher maximum ON current, while the OFF current is preserved. These observations are in agreement with a reduction in the density of the interfacial traps, as evidenced by the estimation performed from SS. Remarkably, the device mobility becomes channel length independent after doping, hinting that the performance of pristine devices are severely limited by contact resistance. A detailed KPFM characterization of the devices in operando demonstrates that indeed an important reduction of R_c is taking place after their treatment with the iodine solution, reaching almost ohmic contact. The results indicate that the aqueous iodine solution route yields a metal–semiconductor interface that is much more favorable to injection and extraction.

This work contributes with a new doping strategy for controlling the electrical properties of OFETs, which results in an important decrease in the device contact resistance, one of the main figures of merit that is at the focus of current interest to realize high frequency devices.[55,56]

4. Experimental Section

Device Preparation: C8-BTBT-C8 and polystyrene $M_w = 10\,000$ Kg mol^{-1} were purchased from Sigma–Aldrich and used without further purification. A blend solution of C8-BTBT-C8 and PS in chlorobenzene 2 wt.% was prepared at weight ratio C8-BTBT-C8:PS 4:1. The blend films were deposited by the BAMS technique in ambient conditions at 105 °C and at a coating speed of 10 mm s^{-1}, as previously reported.[4] The same procedure was applied for diF-TES-ADT (purchased from Lumtec) and TIPS-pentacene (purchased from Ossila). Si/SiO_2 substrates were purchased from Si-Mat (SiO_2 thickness was 200 nm, $C = 17.26 \times 10^{-9}$ F cm^{-2}) and were cleaned by acetone and isopropanol and dried under a nitrogen flow. Top source–drain electrodes consisting 25 nm of Au were thermally evaporated through a shadow mask with channel width W = 4 mm and channel lengths L = 50–200 µm. After evaporation, samples were kept in dark for 7 days.

Doping Process: Iodine solid was purchased from Sigma–Aldrich and used directly. A saturated solution (concentration 0.29 mg mL^{-1}) of iodine and MilliQ water was prepared. This solution was diluted to different decreasing concentrations for performing the experiments related to the influence of iodine concentration on the electrical characteristics. Doping treatment was done by exposing the top surface of the devices to the aqueous iodine solution. A droplet of the solution was casted on the device, completely covering the OFET channel. After 3 min, the device was abundantly washed with MilliQ water and dried with a nitrogen flow. Encapsulation was carried out by spin coating Cytop solution at 3000 rpm min^{-1}.

Electrical Measurements: The electrical measurements were performed in ambient conductions using an Agilent B1500A semiconductor devices analyzer connected to the samples with a Karl Suss probe station. Transfer characteristics were measured in the linear and saturation regime. The mobility was extracted for linear regime and saturation regime using the following equations:

$$\mu_{lin} = \frac{L}{WCV_D}\frac{\partial |I_D|}{\partial V_G} \quad \mu_{sat} = \frac{2L}{WC}\left(\frac{\partial \sqrt{|I_D|}}{\partial V_G}\right)^2 \tag{2}$$

The threshold voltage (V_{th}) was extracted with the equations,

$$I_D = \frac{W}{L}\mu C(V_G - V_{th})V_D \qquad I_D = \frac{W}{2L}\mu C(V_G - V_{th})^2 \tag{3}$$

where C is the insulator capacitance per unit area (C = 17.26 nF cm^{-2}) and W and L are the width and length of the channel, respectively.

Polarized Optical Microscopy: Polarized optical microscopy images were taken with Olympus BX51 microscope equipped with polarizer and analyzer at 90° in reflection mode.

X-Ray: X-ray specular diffractograms in the 2θ range 2.5–30° were collected on a Siemens D-5000 diffractometer.

UV–vis–NIR Spectroscopy: The absorption spectrum of the films was measured by a UV–vis spectrophotometer (V-780).

UV-Resonant Raman: UVRR spectra were measured at the Elettra Synchrotron radiation facility in Trieste, employing the same experimental setup adopted in reference.[57] An excitation wavelength from a diode laser tuned at 266 nm has been used.

Atomic Force Microscopy and Kelvin Probe Force Microscopy: AFM and KPFM data were acquired using a commercial head and control electronics from Nanotec Electronica. Conducting CrPt-coated Si tips mounted on rectangular cantilevers from BudgetSensors, with nominal force constant k = 3 N m^{-1} and 75 kHz of resonance frequency, were used. KPFM was employed in the frequency modulation (FM) mode to measure local surface contact potential differences (SP) on the devices under operation conditions. During FM-KPFM measurements, the tip is excited by an ac voltage (≈0.5 V) at a given frequency ($f_{ac} \approx 0.7$ kHz) while a feedback loop adjusts the dc bias needed to nullify the frequency shift (Δf) of the mechanical oscillation, which is proportional to the electrostatic force gradient. In our setup, the voltage is applied to the tip so that the higher the surface potential the lower the work function (ϕ). SP maps were obtained simultaneously with topography in a single pass mode. The OFETs were mounted in the AFM and were operated and measured with two Keithley 2450 system source-meter instruments. All presented images were analyzed by using the WSxM freeware.[58]

Supporting Information

Supporting Information is available from the Wiley Online Library or from the author.

Acknowledgements

This work was funded by the Spanish Ministry with the project GENESIS PID2019-111682RB-I00, PID2019-110907GB-I00, MAT2017-85089-C2-1-R (AEI/FEDER, UE) and through the "Severo Ochoa" Programme for Centers of Excellence in R&D (FUNFUTURE CEX2019-000917-S) and the Generalitat de Catalunya (2017-SGR-918). T. S. and F. D. acknowledge CERIC-ERIC for providing access to the Elettra IUVS-OFF beamline (beamtime number 20187028). J. L. acknowledges the Scholarship from the Chinese Council and J. L. and A. B. are enrolled in the UAB Materials Science PhD program. A.B. thanks the Spanish Government financial support through BES-2016-077519 FPI fellowship.

Conflict of Interest

The authors declare no conflict of interest.

Data Availability Statement

The data that support the findings of this study are available from the corresponding author upon reasonable request.

Keywords

aqueous iodine solution, contact resistance, chemical doping, Kelvin Probe Microscopy, OFET

Received: November 19, 2021
Revised: January 16, 2022
Published online: February 12, 2022

[1] M. Mas-Torrent, C. Rovira, *Chem. Soc. Rev.* **2008**, *37*, 827.
[2] S. Z. Dawson, RM, D. A. Furst, S. Connor, J. Hsu, M. G. Kane, R. G Stewart, A. Ipri, C. N. King, P. J. Green, R. Y. Flegal, *in SID Symp. Digest Tech. Papers* **1998**, *29*, 11.
[3] J. W. Rumer, I. McCulloch, *Mater. Today* **2015**, *18*, 425.
[4] I. Temiño, F. G. Del Pozo, M. R. Ajayakumar, S. Galindo, J. Puigdollers, M. Mas-Torrent, *Adv. Mater. Technol.* **2016**, *1*, 1600090.
[5] H. T. Yi, M. M. Payne, J. E. Anthony, V. Podzorov, *Nat. Commun.* **2012**, *3*, 1259.
[6] A. F. Paterson, S. Singh, K. J. Fallon, T. Hodsden, Y. Han, B. C. Schroeder, H. Bronstein, M. Heeney, I. McCulloch, T. D. Anthopoulos, *Adv. Mater.* **2018**, *30*, 1801079.
[7] C. Liu, Y. Li, T. Minari, K. Takimiya, K. Tsukagoshi, *Org. Electron.* **2012**, *13*, 1146.
[8] S. Galindo, A. Tamayo, F. Leonardi, M. Mas-Torrent, *Adv. Funct. Mater.* **2017**, *27*, 1700526.

[9] J. W. Borchert, R. T. Weitz, S. Ludwigs, H. Klauk, *Adv. Mater.* **2021**, https://doi.org/10.1002/adma.202104075e2104075.
[10] C. Liu, Y. Xu, Y.-Y. Noh, *Mater. Today* **2015**, *18*, 79.
[11] M. Waldrip, O. D. Jurchescu, D. J. Gundlach, E. G. Bittle, *Adv. Funct. Mater.* **2019**, *30*, 1904576.
[12] Y. Gao, Y. Shao, L. Yan, H. Li, Y. Su, H. Meng, X. Wang, *Adv. Funct. Mater.* **2016**, *26*, 4456.
[13] K. C. Roh J, J Kwak, C Lee, B. Jun Jung, *Appl. Phys. Lett.* **2014**, *104*, 103303.
[14] Y. Mei, D. Fogel, J. Chen, J. W. Ward, M. M. Payne, J. E. Anthony, O. D. Jurchescu, *Org. Electron.* **2017**, *50*, 100.
[15] H. F. Haneef, A. M. Zeidell, O. D. Jurchescu, *J. Mater. Chem. C* **2020**, *8*, 759.
[16] A. Campos, S. Riera-Galindo, J. Puigdollers, M. Mas-Torrent, *ACS Appl. Mater. Interfaces* **2018**, *10*, 15952.
[17] R. Meerheim, C. Körner, K. Leo, *Appl. Phys. Lett.* **2012**, *100*, 59.
[18] G. Adamopoulos, S. Thomas, P. H. Wobkenberg, D. D. Bradley, M. A. McLachlan, T. D. Anthopoulos, *Adv. Mater.* **2011**, *23*, 1894.
[19] I. E. Jacobs, A. J. Moule, *Adv. Mater.* **2017**, *29*, 1703063.
[20] S. Reineke, F. Lindner, G. Schwartz, N. Seidler, K. Walzer, B. Lussem, K. Leo, *Nature* **2009**, *459*, 234.
[21] R. Meerheim, C. Körner, K. Leo, *Appl. Phys. Lett.* **2014**, *105*, 063306.
[22] B. Lüssem, M. Riede, K. Leo, *Phys. Status Solidi* **2013**, *210*, 9.
[23] K. Walzer, B. Maennig, M. Pfeiffer, K. Leo, *Chem. Rev.* **2007**, *107*, 1233.
[24] A. Babuji, I. Temino, A. Perez-Rodriguez, O. Solomeshch, N. Tessler, M. Vila, J. Li, M. Mas-Torrent, C. Ocal, E. Barrena, *ACS Appl. Mater. Interfaces* **2020**, *12*, 28416.
[25] M. L. Tietze, J. Benduhn, P. Pahner, B. Nell, M. Schwarze, H. Kleemann, M. Krammer, K. Zojer, K. Vandewal, K. Leo, *Nat. Commun.* **2018**, *9*, 1182.
[26] A. Perez-Rodriguez, I. Temino, C. Ocal, M. Mas-Torrent, E. Barrena, *ACS Appl. Mater. Interfaces* **2018**, *10*, 7296.
[27] A. D. Scaccabarozzi, F. Scuratti, A. J. Barker, A. Basu, A. F. Paterson, Z. Fei, O. Solomeshch, A. Petrozza, N. Tessler, M. Heeney, T. D. Anthopoulos, M. Caironi, *Adv. Electron. Mater.* **2020**, *6*, 2000539.
[28] J. Panidi, A. F. Paterson, D. Khim, Z. Fei, Y. Han, L. Tsetseris, G. Vourlias, P. A. Patsalas, M. Heeney, T. D. Anthopoulos, *Adv. Sci.* **2018**, *5*, 1700290.
[29] A. F. Paterson, Y.-H. Lin, A. D. Mottram, Z. Fei, M. R. Niazi, A. R. Kirmani, A. Amassian, O. Solomeshch, N. Tessler, M. Heeney, T. D. Anthopoulos, *Adv. Electron. Mater.* **2018**, *4*, 1700464.
[30] Y. Zhang, B. de Boer, P. W. M. Blom, *Adv. Funct. Mater.* **2009**, *19*, 1901.
[31] B. H. Lee, G. C. Bazan, A. J. Heeger, *Adv. Mater.* **2016**, *28*, 57.
[32] B. Lussem, C. M. Keum, D. Kasemann, B. Naab, Z. Bao, K. Leo, *Chem. Rev.* **2016**, *116*, 13714.
[33] Q. Zhang, F. Leonardi, S. Casalini, M. Mas-Torrent, *Adv. Funct. Mater.* **2017**, *27*, 1703899.
[34] H. Minemawari, T. Yamada, H. Matsui, J. Tsutsumi, S. Haas, R. Chiba, R. Kumai, T. Hasegawa, *Nature* **2011**, *475*, 364.
[35] A. F. Paterson, N. D. Treat, W. Zhang, Z. Fei, G. Wyatt-Moon, H. Faber, G. Vourlias, P. A. Patsalas, O. Solomeshch, N. Tessler, M. Heeney, T. D. Anthopoulos, *Adv. Mater.* **2016**, *28*, 7791.
[36] K. Haase, C. Teixeira da Rocha, C. Hauenstein, Y. Zheng, M. Hambsch, S. C. B. Mannsfeld, *Adv. Electron. Mater.* **2018**, *4*, 1800076.
[37] J. Soeda, Y. Hirose, M. Yamagishi, A. Nakao, T. Uemura, K. Nakayama, M. Uno, Y. Nakazawa, K. Takimiya, J. Takeya, *Adv. Mater.* **2011**, *23*, 3309.
[38] K. Pei, A. H. Y. Lau, P. K. L. Chan, *Phys. Chem. Chem. Phys.* **2020**, *22*, 7100.
[39] Q. J. He D, L. Zhang, J. Wang, T. Lan, J. Qian, Y. Li, Y. Shi, Y. Chai, W. Lan, L. K. Ono, *Sci. Adv.* **2017**, *3*, 1701186.
[40] F. G. del Pozo, S. Fabiano, R. Pfattner, S. Georgakopoulos, S. Galindo, X. Liu, S. Braun, M. Fahlman, J. Veciana, C. Rovira, X. Crispin, M. Berggren, M. Mas-Torrent, *Adv. Funct. Mater.* **2016**, *26*, 2379.
[41] T. Izawa, E. Miyazaki, K. Takimiya, *Adv. Mater.* **2008**, *20*, 3388.
[42] W. Wei, C. Yang, J. Mai, Y. Gong, L. Yan, K. Zhao, H. Ning, S. Wu, J. Gao, X. Gao, G. Zhou, X. Lu, J. M. Liu, *J. Mater. Chem. C* **2017**, *5*, 10652.
[43] M. L. Tietze, P. Pahner, K. Schmidt, K. Leo, B. Lüssem, *Adv. Funct. Mater.* **2015**, *25*, 2701.
[44] C. L. Bentley, A. M. Bond, A. F. Hollenkamp, P. J. Mahon, J. Zhang, *J. Phys. Chem. C* **2015**, *119*, 22392.
[45] J. L. J. J. Dané L M, J. G. Hoogland, *Electrochim. Acta* **1968**, *13*, 507.
[46] Y. Tsutsui, G. Schweicher, B. Chattopadhyay, T. Sakurai, J. B. Arlin, C. Ruzie, A. Aliev, A. Ciesielski, S. Colella, A. R. Kennedy, V. Lemaur, Y. Olivier, R. Hadji, L. Sanguinet, F. Castet, S. Osella, D. Dudenko, D. Beljonne, J. Cornil, P. Samori, S. Seki, Y. H. Geerts, *Adv. Mater.* **2016**, *28*, 7106.
[47] A. Babuji, F. Silvestri, L. Pithan, A. Richard, Y. H. Geerts, N. Tessler, O. Solomeshch, C. Ocal, E. Barrena, *ACS Appl. Mater. Interfaces* **2020**, *12*, 57578.
[48] K. Takimiya, I. Osaka, T. Mori, M. Nakano, *Accounts Chem. Res.* **2014**, *47*, 1493.
[49] H. Ebata, T. Izawa, E. Miyazaki, K. Takimiya, M. Ikeda, H. Kuwabara, T. Yui, *J. Am. Chem. Soc.* **2007**, *129*, 15732.
[50] F. Otón, R. Pfattner, E. Pavlica, Y. Olivier, E. Moreno, J. Puigdollers, G. Bratina, J. Cornil, X. Fontrodona, M. Mas-Torrent, J. Veciana, C. Rovira, *Chem. Mater.* **2010**, *23*, 851.
[51] C. Liu, Y. Xu, Y. Li, W. Scheideler, T. Minari, *J. Phys. Chem. C* **2013**, *117*, 12337.
[52] A. F. Paterson, A. D. Mottram, H. Faber, M. R. Niazi, Z. Fei, M. Heeney, T. D. Anthopoulos, *Adv. Electron. Mater.* **2019**, *5*, 1800723.
[53] O. L. Griffith, J. E. Anthony, A. G. Jones, D. L. Lichtenberger, *J. Am. Chem. Soc.* **2010**, *132*, 580.
[54] J. Smith, R. Hamilton, Y. Qi, A. Kahn, D. D. C. Bradley, M. Heeney, I. McCulloch, T. D. Anthopoulos, *Adv. Funct. Mater.* **2010**, *20*, 2330.
[55] U. Zschieschang, J. W. Borchert, M. Giorgio, M. Caironi, F. Letzkus, J. N. Burghartz, U. Waizmann, J. Weis, S. Ludwigs, H. Klauk, *Adv. Funct. Mater.* **2019**, *30*, 1903812.
[56] A. Perinot, M. Giorgio, V. Mattoli, D. Natali, M. Caironi, *Adv. Sci.* **2021**, *8*, 2001098.
[57] T. Salzillo, F. D'Amico, N. Montes, R. Pfattner, M. Mas-Torrent, *CrystEngComm* **2021**, *23*, 1043.
[58] I. F. Horcas, R, J. M. Gomez-Rodriguez, JW Colchero, JW Gómez-Herrero, AM. Baro, *Rev. Sci. Instrum.* **2007**, *78*, 013705.